

# On the study of mixing and drying on electrochemical performance of spinel $\text{LiMn}_2\text{O}_4$ cathodes

Cite as: J. Renewable Sustainable Energy **11**, 014104 (2019); <https://doi.org/10.1063/1.5051583>  
Submitted: 10 August 2018 . Accepted: 18 January 2019 . Published Online: 06 February 2019

Pura Ram, Harish Patel, Rahul Singhal, Ganpat Choudhary, and Rakesh K. Sharma



View Online



Export Citation



CrossMark

## ARTICLES YOU MAY BE INTERESTED IN

[Numerical study on the effect of bi-polar plate geometry in the SOFC heating-up process](#)

Journal of Renewable and Sustainable Energy **11**, 014301 (2019); <https://doi.org/10.1063/1.5047278>

[Clustering-based computation of degradation rate for photovoltaic systems](#)

Journal of Renewable and Sustainable Energy **11**, 014701 (2019); <https://doi.org/10.1063/1.5042688>

[State of charge and state of power management of the hybrid energy storage system in an architecture of microgrid](#)

Journal of Renewable and Sustainable Energy **11**, 014103 (2019); <https://doi.org/10.1063/1.5053567>

Don't let your writing  
keep you from getting  
published!

AIP | Author Services

Learn more today!



# On the study of mixing and drying on electrochemical performance of spinel $\text{LiMn}_2\text{O}_4$ cathodes

Cite as: J. Renewable Sustainable Energy **11**, 014104 (2019); doi: 10.1063/1.5051583

Submitted: 10 August 2018 · Accepted: 18 January 2019 ·

Published Online: 6 February 2019



Pura Ram,<sup>1</sup> Harish Patel,<sup>1</sup> Rahul Singhal,<sup>2</sup> Ganpat Choudhary,<sup>1</sup> and Rakesh K. Sharma<sup>1,a)</sup>

## AFFILIATIONS

<sup>1</sup>Department of Chemistry, Indian Institute of Technology Jodhpur, Jodhpur 342037, Rajasthan, India

<sup>2</sup>Department of Physics and Engineering Physics, Central Connecticut State University, New Britain, Connecticut 06050, USA

<sup>a)</sup>Email: rks@iitj.ac.in

## ABSTRACT

The current work presents the effect of stirring hours and drying temperature on the quality of slurry, its surface morphology, and electrochemical performances of electrodes. Physical characterization studies, such as XRD, SEM, and SEM of slurry, and electrochemical characterization studies, namely, the investigation of charge-discharge capacities, rate performances, cyclability, and AC-impedance, were carried out. The cathode slurry was prepared at four different stirring intervals of 3 h, 4 h, 5 h, and 6 h and six different drying temperatures of 80, 90, 100, 110, 120, and 130 °C. The results showed that slurry obtained at a stirring time of 5 h and at a drying temperature of 120 °C exhibited best physical and electrochemical performances. SEM images showed that slurry obtained at a stirring time of 5 h has better surface uniformity and homogeneity compared to others. The electrodes prepared from this slurry also showed improved charge-discharge capacity and rate performance and low impedance. The initial discharge capacities of the electrodes, made from slurry with stirring times of 4 h, 5 h, and 6 h, were 54, 73, and 58  $\text{mAhg}^{-1}$ , respectively at a current rate of  $C/10$ . The current study also provides clear-cut outline steps to prepare good quality cathode slurry. This study may provide guidelines for new researchers in the field of Li-ion battery technology to overcome these issues and get first hand good quality slurry for better results.

Published under license by AIP Publishing. <https://doi.org/10.1063/1.5051583>

## I. INTRODUCTION

Spinel cathode  $\text{LiMn}_2\text{O}_4$  and layered  $\text{LiCoO}_2$  based Li-ion battery materials have been studied over the past 2–3 decades. The supportive features such as high open circuit voltage, high energy and power density, and low toxicity and cost of  $\text{LiMn}_2\text{O}_4$  over the layered  $\text{LiCoO}_2$  have made it the forefront runner and leader to supply future generation energy storing technology.<sup>1–6</sup> The major research concern is to find a novel and stable cathode material for energy storage. These cathode materials include doped cathodes, transition metal (Fe, Zn, Co, Al, and Mg) doped cathodes,<sup>7–11</sup> rare-earth doped (Nd, Gd, Dy, Tb, and Sm) cathodes,<sup>12–16</sup> dual metal doped (Gd + Co) cathodes,<sup>11</sup> transition metal and non-metal doped (Mg-F) cathodes,<sup>17</sup> metal oxide coated cathode  $\text{ZrO}$ ,<sup>18</sup> and alternate cathode  $\text{LiFePO}_4$ <sup>19</sup> for making lithium ion based rechargeable battery technology viable and economical. The cathode is considered as current capacity

determining part of batteries. Other parts of batteries, anode, separator, electrolyte, and packaging material, play an equivalent role in making the technology marketable. The fabrication of the cathode involves a cathode material (CM), carbon black (CB) as a conductive agent, and a binder (PVDF) and also involves slurry process steps. However, less attention was paid towards the slurry process optimization based on the stirring duration.

The cathode fabrication process can be categorised into three parts: (a) slurry processes (mixing of raw materials), (2) coating and drying, and (3) cutting of electrodes.<sup>20</sup> The slurry process contains the optimization of the amount of CM, CB, PVDF, and solvent (NMP), its mixing sequence and loading rate, stirring rate, RPM, and duration of stirring. The next steps are the coating strategy, determination of drying temperature and its duration, calendaring, and cathode cutting method. Researchers reported that battery performance was affected by the sequence of mixing and rheological properties; viscosity,

fluid flow, and visco-elasticity;<sup>21–23</sup> electrode thickness,<sup>24</sup> immiscible fluid mixing (water in organic solvent),<sup>25</sup> dispersion of solid ingredients during the slurry process using dispersion agents,<sup>26</sup> length of uniform loading,<sup>27</sup> material phase formation,<sup>28</sup> material loading rate,<sup>29</sup> amount of carbon black and polyvinylidene difluoride (PVDF) binder,<sup>30</sup> styrene butadiene rubber (SBR) binder in aqueous medium, particle size dependent homogeneity,<sup>31</sup> and energy impact of the drying process.<sup>32</sup> The slurry quality based on NMP solvent assessed by AC impedance spectroscopy showed the large variation of 300  $\Omega$  to 3000  $\Omega$  in the internal impedance of the cell.<sup>33</sup> The effect of these parameters was not found in a single study as cumulative in the literature survey.

The current work presents the effect of the drying temperature and stirring duration at fixed RPM on spinel cathode  $\text{LiMn}_2\text{O}_4$ . The influence is assessed through the study of the surface morphology, cyclic voltammetry, charge-discharge studies, and AC impedance analysis. This study provides an easy path for slurry preparation including straightforward steps to assist new researchers in this field.

## II. EXPERIMENTAL SECTION

### A. Active material synthesis

The analytical grade chemical reagents, lithium acetate dihydrate ( $\text{LiOOCCH}_3 \cdot 2\text{H}_2\text{O}$ ) and manganese acetate tetrahydrate [ $\text{Mn}(\text{OOCCH}_3)_2 \cdot 4\text{H}_2\text{O}$ ], all from Alfa Aesar, were taken at a stoichiometric ratio of 1:2. Each constituent was dissolved homogeneously in 2-ethylhexanoic acid as a solvent with magnetic beads and stirred at 300 rpm for  $\sim 1$  h. Both the solutions were mixed and kept at 250  $^\circ\text{C}$  until converted into semi-viscous gel. The magnetic bead was taken out and heated continuously, till gel converted into blackish-brownish powder. The obtained powder was manually ground for half an hour and pyrolyzed in a box furnace (Nabertherm GmbH, Germany), at 450  $^\circ\text{C}$  for 4 h to remove organic impurities. To get the phase pure spinel cathode, the powder was again heated at 850  $^\circ\text{C}$  for 14 h with two steps, at rates of 6.83  $^\circ\text{C}/\text{min}$  (up to 500  $^\circ\text{C}$ ) and 3.33  $^\circ\text{C}/\text{min}$  (500 to 800  $^\circ\text{C}$ ). The resultant powder was ground for 10 min manually in an agate mortar pestle.

### B. Active powder characterization

An X-ray diffractometer, a scanning electron microscope, and an energy dispersive X-ray spectrometer were used for physical characterization of the synthesized battery grade

powder. X-ray diffraction studies were performed on a Bruker D8 advance, at two theta angles in-between 10 $^\circ$ –80 $^\circ$  with a scan rate of 1 $^\circ$  per minute in the locked coupled mode. The surface morphology and elemental analysis were studied by Scanning Electron Microscopy (SEM) using Carl Zeiss, Evo special addition and attached with EDX (OXFORD Instruments). The beam current during surface morphology and energy dispersive X-ray studies was 80 pA and 200 nA, respectively.

### C. Cathode slurry preparation

The cathode slurry was prepared by taking 160 mg of active materials ( $\text{LiMn}_2\text{O}_4$ ), 20 mg of C-black (Alfa Aesar), 20 mg of polyvinylidene difluoride (PVDF, Alfa Aesar), and 600  $\mu\text{l}$  of N-methylpyrrolidone (NMP), Alfa Aesar. The slurry preparation was completed in two steps as shown in Fig. 1. In the first step, the homogeneous solution of PVDF in N-methylpyrrolidone was obtained, and in the second step, the dry mixture of active materials and C-black was poured slowly into the resultant homogeneous solution of the first step ensuring the continuous stirring at 400 rpm. After complete homogenization of the dry mixture in solvent, the slurry was continuously stirred for a duration of 3–6 h at 800 rpm. The slurry was prepared in different two sets of batches T1 to T6 and S1 to S4. The first set of slurry batch (T1 to T6) was stirred for 3 h/800 rpm and dried at 80, 90, 100, 110, 120, and 130  $^\circ\text{C}$  for T1 to T6 batches, respectively, to evaluate the effect of temperature. The second set of slurry batch was dried at 120  $^\circ\text{C}$  and stirred for 3 h, 4 h, 5 h, and 6 h for S1 to S4, respectively.

### D. Cell fabrication and electrochemical characterization

The Al-metal foil coated with wet slurry (for both sets of batches) was kept in an oven for drying at various temperatures of 80, 90, 100, 110, 120, and 130  $^\circ\text{C}$  and time durations of 2–4 h. The dried cathode was cut into a circular shape with a diameter of 8 mm and stored for further use. The other parts of the cell were the anode (Li metal foil, Alfa Aesar, USA), separator [Whatman glass microfiber filters (grade GF/A)], and electrolyte 1M  $\text{LiPF}_6$  into EC + DMC (1:1) of Sigma Aldrich, USA. The two/three connection swagelok cell was assembled in an argon filled glove box; Mbraun, Germany; with  $\text{H}_2\text{O} < 1$  PPM and  $\text{O}_2 < 2$  PPM. Cyclic voltammetry was carried at a scan rate of 0.1 mV/s using a CHI 600 instrument. The galvanostatic charge-discharge studies were performed at different C-rates and up to 10

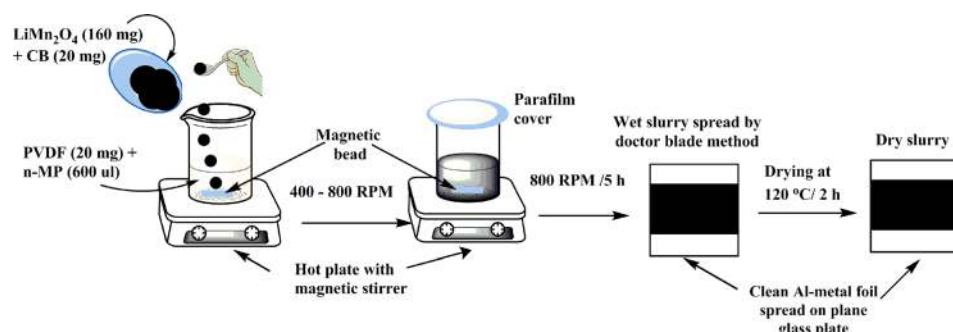
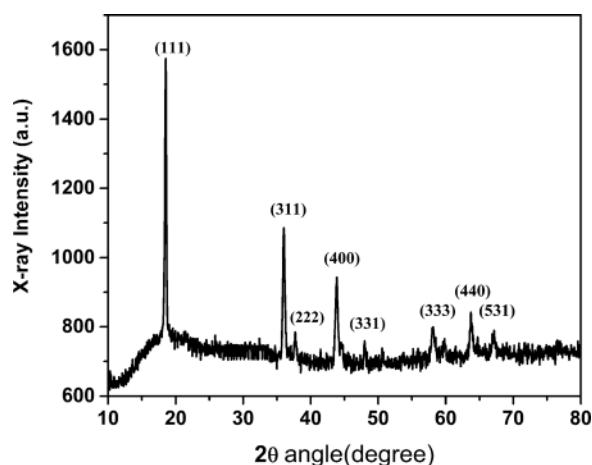


FIG. 1. Schematic of slurry preparation steps for spinel cathode  $\text{LiMn}_2\text{O}_4$ .

FIG. 2. XRD of  $\text{LiMn}_2\text{O}_4$  calcined at  $800^\circ\text{C}$  for 14 h.

Cycles on an 8 channel battery analyzer, MTI Corporation, USA. The AC impedance spectra were recorded from 0.1 MHz to 1 Hz with 0.5 mV AC signals over open circuit potential.

### III. RESULTS AND DISCUSSION

#### A. Structural and surface morphology analyses of the active material

The phase purity of synthesized spinel phase cathode material  $\text{LiMn}_2\text{O}_4$  was assessed using an X-ray diffractometer and is shown in Fig. 2. The crystal structure is well matched with JCPDS file 35-0782.

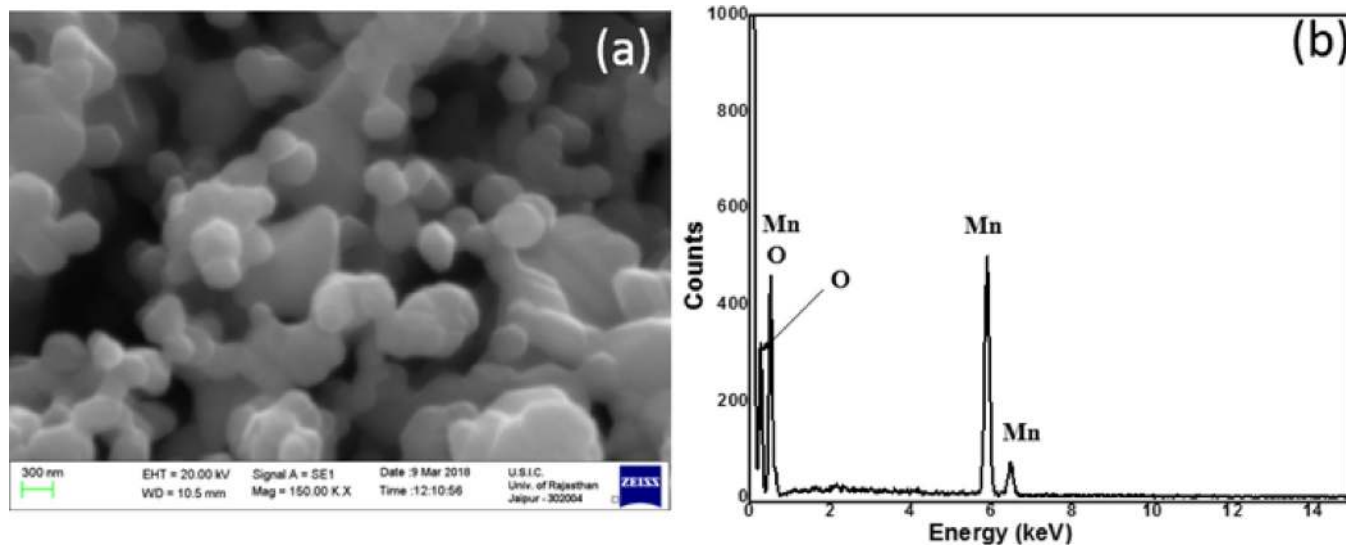
The cubic phase has a space group of  $\text{Fd}3\text{m}$ . The sharp peaks observed in the diffraction pattern are evidenced for better crystallinity and assigned to planes (111), (311), (222), (400),

(311), (511), (440), and (531). The lattice constant and the particle size were found to be  $8.2888\text{ \AA}$ . The occupancy of  $\text{Mn}^{+3}/\text{Mn}^{+4}$  (I311/400) at tetrahedral site proportions was 1.59.

The surface morphology of synthesized  $\text{LiMn}_2\text{O}_4$  cathode powder and its elemental spectra were investigated and are shown in Fig. 3. The particle shapes were irregular polyhedron with different dimensions. The particle size varied from  $1\text{ }\mu\text{m}$  to  $400\text{ nm}$ . The average particle size was  $0.5\text{ }\mu\text{m}$ . The tendency of agglomeration was observed. EXD spectra revealed that elements manganese and oxygen were only observed. It is evidenced that no elemental impurity was formed during the synthesis process. The homogeneity and quality of the prepared slurry following the drying in an  $\text{O}_2$  atmosphere were also investigated by recording the 8 MX picture using a MOTO G2 inbuilt camera to obtain the microscopic view and the SEM images to see the microscopic view as shown in Figs. 4 and 5.

#### B. Macroscopic and microscopic analyses of the prepared slurry

The surface morphology of the prepared slurry was investigated using two mechanisms to obtain qualitative information about the homogeneity. The effect of stirring hours and drying temperature was evidenced that it has more impact on slurry quality which includes homogeneous mixing of the Active material, C-black, and PVDF and smooth surface generation. The stirring speed (rpm) and time (hour) play a vital role in obtaining better quality slurry-gel. The optimized stirring speed and time give the better results compared to other mechanisms. However, the particle size of the active material, carbon black, and PVDF was also the determining factor. A series of experiments were carried out, and the results are presented in Figs. 4 and 5. The macroscopic views of the prepared slurries are presented in Fig. 4 at varying stirring hours from 4, 5, and 6 h and a drying temperature of  $120^\circ\text{C}$ . It is evident that as stirring hours

FIG. 3.  $\text{LiMn}_2\text{O}_4$  calcined at  $800^\circ\text{C}$  for 14 h: (a) surface morphology and (b) EDX elemental spectra.

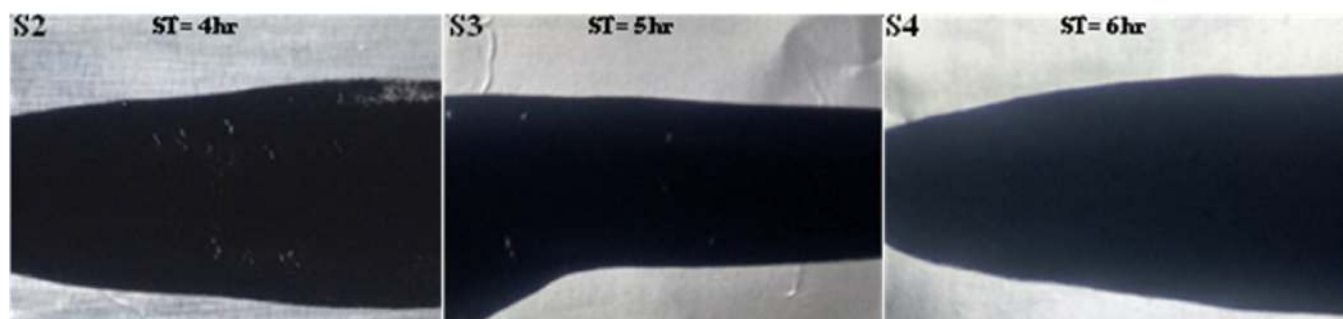


FIG. 4. Macroscopic view of the slurry prepared with different stirring hours (S2) 4 h, (S3) 5 h, and (S4) 6 h.

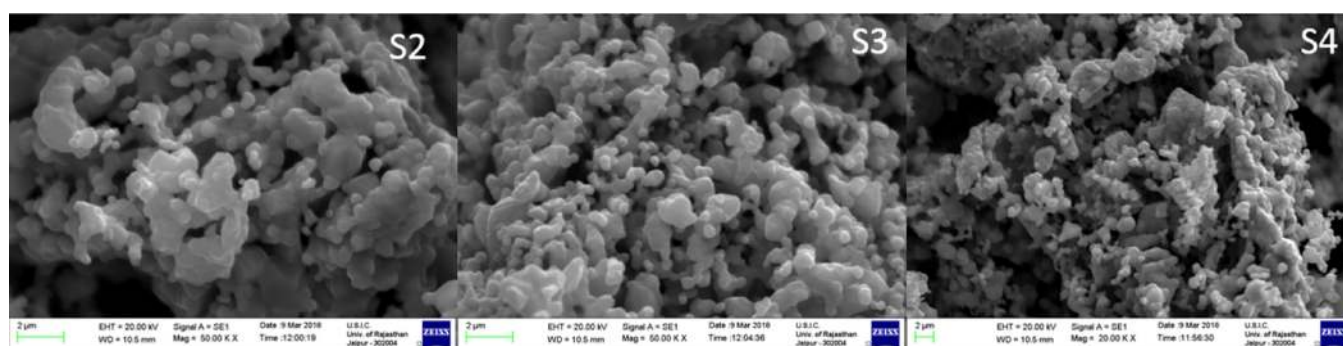


FIG. 5. SEM images of  $\text{LiMn}_2\text{O}_4$  slurry prepared with different stirring hours of (S2) 4 h, (S3) 5 h, and (S4) 6 h.

increase, less cracks are observed, which means that the slurry quality was improved with the increasing stirring hours. For the slurry obtained at a stirring time of 3 h and a drying temperature of  $120^\circ\text{C}$ , a large number of small range cracks appeared and the sample was not further studied. Similarly, the drying temperature less than  $120^\circ\text{C}$  is also responsible for generating cracks.

To get more insight, the surface morphology of these slurries was investigated using scanning electron microscopy as shown in Fig. 4 (S2, S3, and S4). The S3 image indicates that slurry is more uniform and homogenous compared to others S2 and S4. The slurry (S1) was more non-uniform and leached out from Al-foil. The S2 image shows that lumps of active materials and other materials were not mixed properly. It needs more time to obtain a homogeneity of mixtures. Image S4 shows that cracks initiated in slurry. It may be due to breaking and cracking of the cage of the binder on the active material and the carbon-black mixture.

### C. Cyclic voltammetry and C-rate performance

The cyclic voltammograms (CVs) of synthesized spinel cathode  $\text{LiMn}_2\text{O}_4$  were recorded at  $0.1\text{ mV/s}$  for 10 cycles in a potential window of  $3.5\text{--}4.5\text{ V}$ . The cyclic voltammetry of slurry S3 at a scan rate of  $0.1\text{ mV/s}$  for cycles 6–10 is shown in Fig. 6. Similar CVs were observed for slurries S2 and S4 except the variation in the current peak height. The magnitudes of current observed in S3 were  $0.39$  and  $0.21\text{ mA}$ , corresponding to

oxidation potentials of  $4.12\text{ V}$  and  $4.0\text{ V}$  for  $\text{Mn}^{3+} \rightarrow \text{Mn}^{4+}$  at tetrahedral and octahedral sites. More current and intense peaks make the  $\text{Li}^+$  ion intercalation/de-intercalation process easier. The current peak heights remain constant except few initial

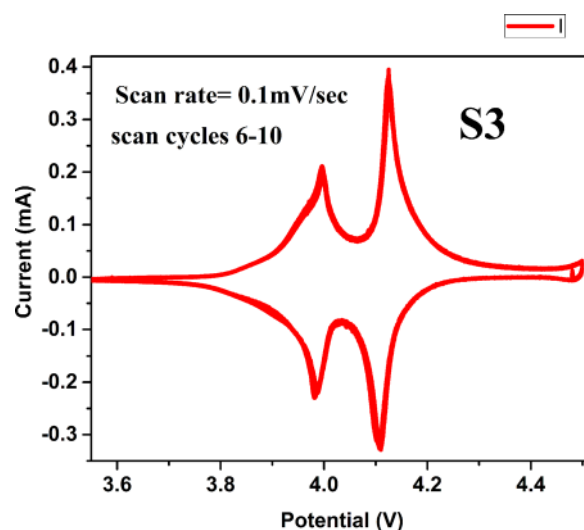


FIG. 6. CV of slurry S3 for  $\text{LiMn}_2\text{O}_4$  at  $0.1\text{ mV/s}$ .

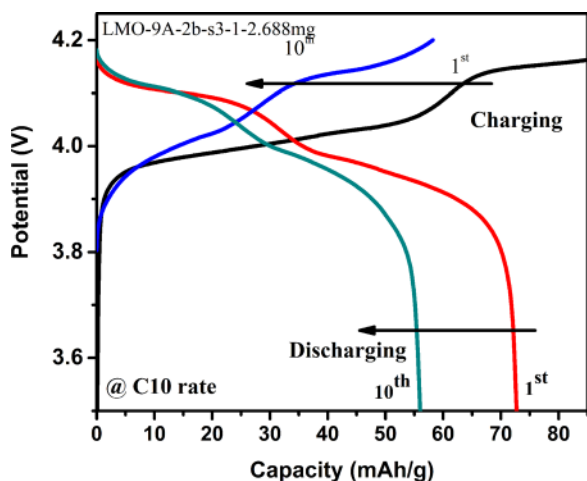


FIG. 7. Charge-discharge curve of slurry S3 for  $\text{LiMn}_2\text{O}_4$  at a current density of C/10.

cycles, which also indicates that there is no increase in electrical resistance during the successive scan cycles.

#### D. Charge-discharge and life cycle performance

The galvanostatic charge-discharge studies were performed for different slurries (S2, S3, and S4) at different C-rates (C/10, C/5, and C/2). Figure 7 shows the 1st and 10th charge-discharge cycles for slurry S3 at the C/10 rate. The initial charge and discharge capacities at the C/10 rate were 85 and 73 mAh/g for slurry S3 which were higher than those of slurries S2 and S4 as shown in Table I. The retention of discharge capacity after performing 10 cycles was 55 mAh/g (75%). Slurry S2 showed low performance at rates of both C10 and C5, while slurry S4 performed intermediate. Also, Fig. 8(a) shows the discharge capacity as a function of stirring time. It can be seen from the figure that the maximum discharge capacity was found for the slurry, obtained after a stirring time of 5 h. These results may be attributed to the improved homogeneity in S4 compared to S2, which is evidenced by SEM slurry images in Fig. 5 (S2 and S4). The less agglomeration and more homogeneity in slurry S3 (Figs. 5 and S3) were powerful features for the improved discharge capacity. The non-uniformity and in-homogeneity of active material distribution in slurry may reduce the  $\text{Li}^+$  diffusion process, which resulted in less capacity of the cathode. It was reported earlier that the solution viscosity drops gradually

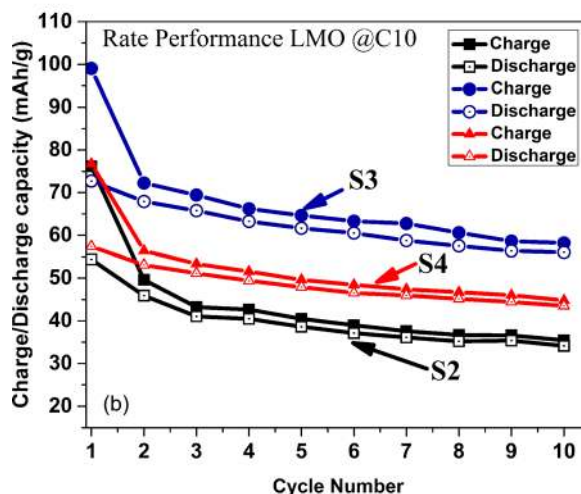
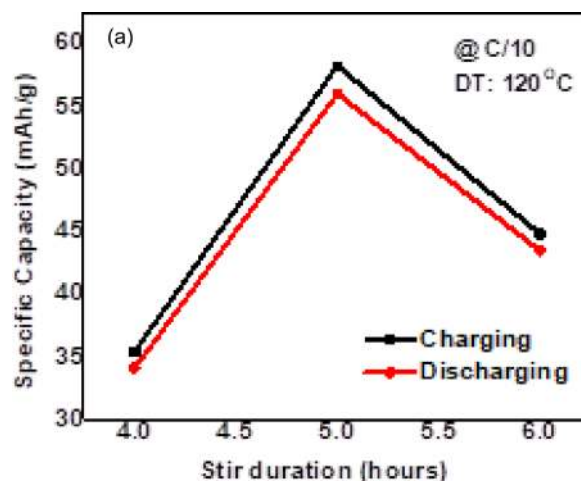


FIG. 8. (a) The specific charge/discharge capacity at the 10th cycle with stirring time. (b) Cycle performance of  $\text{LiMn}_2\text{O}_4$  slurries S2, S3, and S4 at the C/10 rate.

with mixing time and reaches a minimum value after a certain period of mixing. At this point, the particles disperse uniformly into the slurry.<sup>31,34,35</sup> The more homogeneous slurry is free from small air bubbles and provides a smooth and pin hole free coating onto the current collector. This can directly affect the consistency and performance of an electrode's electrochemical behaviour. This might be the reason for better electrode

TABLE I. Charge-discharge performance of cathode slurries at different stirring hours.

Slurry ID	At the C/10 rate				At the C/5 rate			
	Charge capacity ( $\text{mA h g}^{-1}$ )		Discharge capacity ( $\text{mA h g}^{-1}$ )		Charge capacity ( $\text{mA h g}^{-1}$ )		Discharge capacity ( $\text{mA h g}^{-1}$ )	
	1st cycle	10th cycle	1st cycle	10th cycle	1st cycle	10th cycle	1st Cycle	10th Cycle
S2	78	38	54	34	19	17	17	16
S3	85	60	73	55	55	46	49	45
S4	76	45	58	44	40	37	38	35

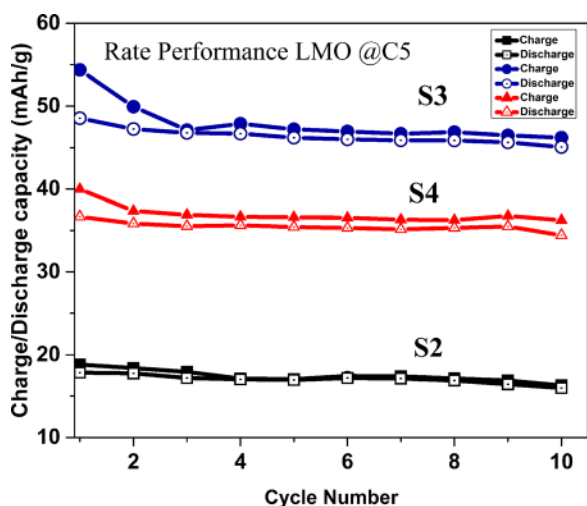


FIG. 9. Cycle performance of  $\text{LiMn}_2\text{O}_4$  slurries S2, S3, and S4 at the C/5 rate.

performance at  $120^\circ\text{C}$  and a stirring time of 5 h. The charge-discharge cycling at the C/5 rate was also investigated, and the results showed almost stable discharge capacity up to 10 cycles. The capacity retention was 91% (45 mAh/g). The cycling behaviour of slurries (S2, S3, and S4) was assessed and is shown in Fig. 8(b) for the C/10 rate and in Fig. 9 for C/5. The capacity loss at C/5 was less compared to that at the C/10 rate up to 10 cycles. All slurries have stable discharge capacity at the C/5 rate with the highest discharge capacity of slurry S3. The more stable discharge capacity at C/5 compared to C/10 also supports the stable lattice structure.

### E. AC impedance analysis

Figure 10 shows the AC impedance of slurry S3 after each CV cycle to understand the impedance build-up after each

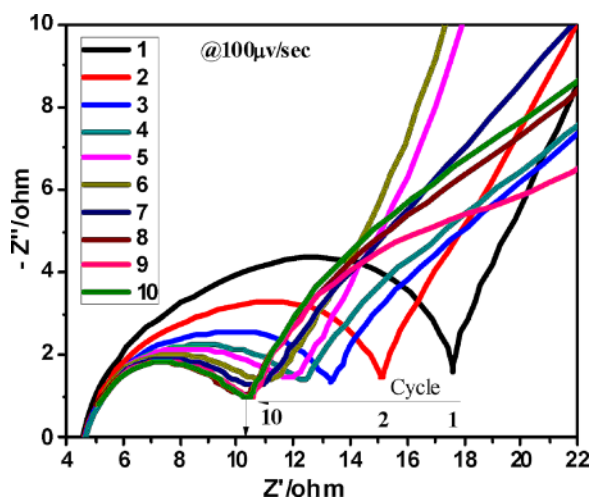


FIG. 10. AC impedance spectra for  $\text{LiMn}_2\text{O}_4$ -S3 slurry.

cycle. The study revealed that initial 4 cycles are sufficient for building up the solid electrolyte interface (SEI) and other polarization effects. After 4 cycles, there is no reduction in electrical impedance, i.e., impedance was saturated and the maximum impedance of the circuit was  $12\ \Omega$  after 10 cycles. It also indicates that reducing the impedance or stabilizing the impedance for the slurry obtained at a stirring time of 5 h and at 800 rpm plays a determining role in slurry preparation. The improved homogeneity and optimized particle size are essential for achieving low impedance and high discharge capacity.

### IV. CONCLUSIONS

Spinel  $\text{LiMn}_2\text{O}_4$  was successfully synthesized via the organic sol-gel route. The effect of stirring hours (3 h, 4 h, 5 h, and 6 h) and drying temperature (80, 90, 100, 110, 120, and  $130^\circ\text{C}$ ) on active cathode slurry at fixed 800 rpm was investigated. The physical characterization showed that pure cubic spinel phase powders were obtained with an average particle size of  $0.5\ \mu\text{m}$ . The cathode slurry (S3) prepared with stirring hours of 5 h at 800 rpm and dried at  $120^\circ\text{C}$  was found to be better than S2 (4 h), S4 (6 h), and others. Slurry S3 (5 h) has the highest initial charge-discharge capacity of 85 and  $73\ \text{mAhg}^{-1}$  at the C/10 rate among all slurries. The discharge capacity and capacity retention were high in S3, compared to S4 and S2. The low AC impedance of  $12\ \Omega$  for S3 revealed that more homogeneity needed an appropriate time of stirring during the slurry process. Thus, the slurry obtained at a stirring time of 5 h at 800 rpm and a drying temperature of  $120^\circ\text{C}$  may be used further to prepare better quality slurry of the cathode materials.

### ACKNOWLEDGMENTS

Dr. Pura Ram acknowledges MHRD, Government of India, for providing financial assistance during research. The authors are also thankful to DST, Government of India, for research support under the Indo-Portuguese bilateral research program (INT/Portugal/P-02/2013; 2014–2016). The authors thank the CASE facility, IIT Jodhpur, for SEM and electrochemical analysis.

### REFERENCES

- <sup>1</sup>J. B. Goodenough and Y. Kim, *Chem. Mater.* **22**(3), 587–603 (2010).
- <sup>2</sup>N. Nitta, F. Wu, J. T. Lee, and G. Yushin, *Mater. Today* **18**(5), 252–264 (2015).
- <sup>3</sup>M. Winter and R. J. Brodd, *Chem. Rev.* **104**(10), 4245–4269 (2004).
- <sup>4</sup>J. W. Fergus, *J. Power Sources* **195**(4), 939–954 (2010).
- <sup>5</sup>M. M. Thackeray, C. Wolverton, and E. D. Isaacs, *Energy Environ. Sci.* **5**, 7854–7863 (2012).
- <sup>6</sup>M. Armand and J. M. Tarascon, *Nature* **451**, 652–657 (2008).
- <sup>7</sup>R. Singhal, S. R. Das, M. S. Tomar, O. Ovideo, S. Nieto, R. E. Melgarejo, and R. S. Katiyar, *J. Power Sources* **164**(2), 857–861 (2007).
- <sup>8</sup>D. Arumugam, G. P. Kalignan, K. Vediappan, and C. W. Lee, *Electrochim. Acta* **55**(28), 8439–8444 (2010).
- <sup>9</sup>L. Xiong, Y. Xu, T. Tao, and J. B. Goodenough, *J. Power Sources* **199**, 214–219 (2012).
- <sup>10</sup>K. Suryakala, K. R. Marikkannu, G. P. Kalignan, and T. Vasudevan, *Int. J. Electrochem. Sci.* **3**(2), 136–144 (2008).
- <sup>11</sup>X. Sun, X. Hu, Y. Shi, S. Li, and Y. Zhou, *Solid State Ionics* **180**(4–5), 377–380 (2009).

- <sup>12</sup>D. K. Lee, M. Pyo, S. C. Han, D. Ahn, S. P. Singh, and K. Sohn, *ACS Appl. Mater. Interfaces* **4**(12), 6842–6848 (2012).
- <sup>13</sup>S. C. Han, B. K. Park, S. P. Singh, K. Sohn, Y. Hwang, M. Pyo, and E. G. Bae, *J. Electrochem. Soc.* **159**(11), A1867–A1873 (2012).
- <sup>14</sup>S. Balaji, T. Mani Chandran, and D. Mutharasu, *Ionics* **18**(6), 549–558 (2012).
- <sup>15</sup>P. Ram, A. Goren, S. Ferdov, M. Silva, R. Singhal, C. M. Costa, R. K. Sharma, and S. Lancers-Mendez, *New J. Chem.* **40**, 6244–6252 (2016).
- <sup>16</sup>D. Liu, X. Liu, and Z. He, *J. Alloys Compd.* **436**(1–2), 387–391 (2007).
- <sup>17</sup>W. Wen, B. Ju, X. Wang, C. Wu, H. Shu, and X. Yang, *Electrochim. Acta* **147**, 271–278 (2014).
- <sup>18</sup>R. Singhal, M. S. Tomar, J. G. Burgos, and R. S. Katiyar, *J. Power Sources* **183**(1), 334–338 (2008).
- <sup>19</sup>A. K. Padhi, K. S. Nanjundaswamy, and J. B. Goodenough, *J. Electrochem. Soc.* **144**(4), 1188–1194 (1997).
- <sup>20</sup>H. Y. Tran, G. Greco, C. Täubert, M. Wohlfahrt-Mehrens, W. Haselrieder, and A. Kwade, *J. Power Sources* **210**, 276–285 (2012).
- <sup>21</sup>K. M. Kim, W. S. Jeon, I. J. Chung, and S. H. Chan, *J. Power Sources* **83**(1–2), 108–113 (1999).
- <sup>22</sup>W. Lee, J. H. Ryu, W. Han, K. H. Ahn, and S. M. Oh, *J. Power Sources* **195**(18), 6049–6054 (2010).
- <sup>23</sup>D. Liu, L.-C. Chen, T. J. Liu, T. Fan, E. Y. Tsou, and C. Tiu, *Adv. Chem. Eng. Sci.* **4**, 515–528 (2014).
- <sup>24</sup>M. Singh, J. Kaiser, and H. Hahn, *J. Electrochem. Soc.* **162**(7), A1196–A1201 (2015).
- <sup>25</sup>B. Bitsch, J. Dittmann, M. Schmitt, P. Scharfer, W. Schabel, and N. Willenbacher, *J. Power Sources* **265**, 81–90 (2014).
- <sup>26</sup>W. Zhang, X. He, W. Pu, J. Li, and C. Wan, *Ionics* **17**(5), 473–477 (2011).
- <sup>27</sup>G. Nagasubramanian, *Int. J. Electrochem. Sci.* **2**(12), 913–922 (2007).
- <sup>28</sup>N. Santander, S. R. Das, S. B. Majumder, and R. S. Katiyar, *Surf. Coat. Technol.* **177–178**, 60–64 (2004).
- <sup>29</sup>P. R. Dasa, L. Komsyyskaa, O. Ostera, and G. Wittstock, *Synth. Met.* **215**, 86–94 (2016).
- <sup>30</sup>G. Liu, H. Zheng, A. S. Simens, A. M. Minor, X. Song, and V. S. Battaglia, *J. Electrochem. Soc.* **154**(12), A1129–A1134 (2007).
- <sup>31</sup>A. Ponrouch and M. R. Palacín, *J. Power Sources* **196**(22), 9682–9688 (2011).
- <sup>32</sup>S. Ahmed, P. A. Nelson, K. G. Gallagher, and D. W. Dees, *J. Power Sources* **322**, 169–178 (2016).
- <sup>33</sup>P. Ram, R. Sinhal, and R. K. Sharma, *Adv. Electrochem.* **2**(1), 46–49 (2014).
- <sup>34</sup>M. Despotopoulou and M. T. Burchill, *Prog. Org. Coat.* **45**, 119–126 (2002).
- <sup>35</sup>Y. Tomita, L. C. Guo, Y. Zhang, N. Uchida, and K. Uematsu, *J. Am. Ceram. Soc.* **78**, 2153–2156 (1995).